

A fully coupled fluid-particle flow solver using quadrature-based moment method with high-order realizable schemes on unstructured grids

V. Vikas^{*}, Z.J. Wang^{*}, A. Passalacqua[†] and R.O. Fox[†]

^{*} Department of Aerospace Engineering, 2271 Howe Hall, Iowa State University, Ames, IA 50011, USA

[†] Department of Chemical and Biological Engineering, 2114 Sweeney Hall, Iowa State University, Ames, IA 50011, USA

vvikas@iastate.edu, zjw@iastate.edu, albertop@iastate.edu and rofox@iastate.edu

Keywords: Kinetic theory of granular flow, QMOM, multiphase flow, unstructured grid, high-order realizable

Abstract

Kinetic Equations containing terms for spatial transport, gravity, fluid drag and particle-particle collisions can be used to model dilute gas-particle flows. However, the enormity of independent variables makes direct numerical simulation of these equations almost impossible for practical problems. A viable alternative is to reformulate the problem in terms of moments of the velocity distribution function. A quadrature method of moments (QMOM) was derived by Desjardins et al. [1] for approximating solutions to the kinetic equation for arbitrary Knudsen number. Fox [2, 13] derived a third-order QMOM for dilute particle flows, including the effect of the fluid drag on the particles. Passalacqua et al. [4] and Garg et al. [3] coupled an incompressible finite-volume solver for the fluid-phase and a third order QMOM solver for particle-phase on Cartesian grids. In the current work a compressible finite-volume fluid solver is coupled with a particle-phase solver based on third-order QMOM on unstructured grids. The fluid and particle-phase are fully coupled by accounting for the volume displacement effects induced by the presence of the particles and the momentum exchange between the phases. The success of QMOM is based on the moment inversion algorithm that allows quadrature weights and abscissas to be computed from the moments of the distribution function. The moment-inversion algorithm does not work if the moments are non-realizable, which might lead to negative weights. Desjardins et al. [1] showed that realizability is guaranteed only with the 1st-order finite-volume scheme that has excessive numerical diffusion. The authors [5, 6] have derived high-order finite-volume schemes that guarantee realizability for QMOM. These high-order realizable schemes are used in this work for the particle-phase solver. Results are presented for a dilute gas-particle flow in a lid-driven cavity with both Stokes and Knudsen numbers equal to 1. For this choice of Knudsen and Stokes numbers, particle trajectory crossing occurs which is captured by QMOM particle-phase solver.

Introduction

Gas-particle flows are relevant in many engineering applications. A detailed understanding of such flows is essential to the improvement of these applications. Currently, there exist several different ways for numerical simulation of gas-particle flows. All of them use the same fluid solver. They differ in the way in which particle phase is treated:

1. Direct solver that discretizes velocity phase space of particle number density function [7, 8].
2. Lagrangian solver that tracks all the particles individually [9].

3. Hydrodynamic models with kinetic theory moment closures [10].

4. Quadrature Method Of Moment (QMOM) solver that solves for moments of particle number density function with quadrature-based closures [1, 2, 4, 11].

A direct solution of the kinetic equation is prohibitively expensive due to the high dimensionality of the space of independent variables, while Lagrangian solvers are computationally very expensive for many engineering and industrial applications, since the number of particles to be tracked is very large. Hydrodynamic models are developed assuming that the Knudsen num-

ber of the flow is nearly zero, which is equivalent to assuming a Maxwellian (or nearly Maxwellian) equilibrium velocity distribution. This, however, is not correct in relatively dilute gas-particle flows, where the Knudsen number is high, the collision frequency is small and phenomena like particle trajectory crossing can happen. In particular, Desjardins et al. [1] showed that the assumption that a gas-particle flow can be described by accounting for only the mean momentum of the particle phase leads to incorrect prediction of all the velocity moments, including the particle number density, showing the need of using a multi-velocity method, in order to correctly capture the physics of the flow.

QMOM for gas particle flow [2, 12, 13] is based on the idea of tracking a set of velocity moments of arbitrarily high order, providing closures to the source terms and the moment spatial fluxes in the moment transport equations by means of a quadrature approximation of the number density function. Fox [2, 13] derived a third order QMOM for dilute particle flows, including the effect of the fluid drag on the particles. Passalacqua et al. [4] and Garg et al. [3] coupled a third order QMOM solver with an incompressible finite volume solver for the fluid-phase on Cartesian grids. In the current work, a compressible finite-volume fluid-phase solver is coupled with a particle phase solver based on third-order QMOM on unstructured grids. The fluid and particle phases are fully coupled by accounting for the volume displacement effects induced by the presence of the particles, and accounting for the momentum exchange between the phases.

The key to the success of QMOM is an inversion algorithm which allows to uniquely determine a set of weights and abscissas from the set of transported moments. Condition for the inversion algorithm to be applied is that the set of moments is realizable, meaning it actually corresponds to a velocity distribution. This condition is not generally ensured by the traditional finite-volume methods used in computational fluid dynamics. Desjardins et al. [1] showed that realizability is guaranteed only with the 1st-order finite-volume scheme. But the 1st-order finite-volume scheme has excessive numerical diffusion. The authors [5, 6] have recently derived high-order finite-volume schemes that guarantee realizability for QMOM. These high-order realizable schemes are used in this work for the particle phase solver.

The remainder of the paper is organized as follows. First the governing equations for the fluid and particle phases are described. Then the details of the two solvers and the coupling algorithm are briefly explained. Finally, numerical results are presented for a dilute gas-particle flow in a lid-driven cavity. For simplicity quantities with subscript f will be associated with fluid-phase. For the particle-phase subscript p may or may not appear

explicitly. Also, any repetition of variable indices will denote summation as per Einstein notation.

Fluid-phase governing equations

The fluid-phase is described by Navier-Stokes equations modified for multi-fluid models. The fluid-phase continuity, momentum and energy equations are given as:

$$\frac{\partial \mathbf{W}_f}{\partial t} + \frac{\partial \mathbf{H}_{ij}(\mathbf{W}_f)}{\partial x_j} = \frac{\partial \mathbf{H}_{ij}^v(\mathbf{W}_f)}{\partial x_j} + \mathbf{S}_f. \quad (1)$$

In (1), \mathbf{W}_f , $\mathbf{H}_{ij}(\mathbf{W}_f)$, $\mathbf{H}_{ij}^v(\mathbf{W}_f)$ and \mathbf{S}_f denote the set of conserved variables, inviscid fluxes, viscous fluxes and source terms respectively. These terms are given by

$$\mathbf{W}_f = \begin{bmatrix} \alpha_f \rho_f \\ \alpha_f \rho_f U_{fi} \\ \alpha_f \rho_f E_f \end{bmatrix}, \quad (2)$$

$$\mathbf{H}_{ij}(\mathbf{W}_f) = \begin{bmatrix} \alpha_f \rho_f U_{fj} \\ \alpha_f (\rho_f U_{fi} U_{fj} + p_f) \\ \alpha_f (\rho_f E_f + p_f) U_{fj} \end{bmatrix}, \quad (3)$$

$$\mathbf{H}_{ij}^v(\mathbf{W}_f) = \begin{bmatrix} 0 \\ \sigma_{fij} \\ \sigma_{fij} U_{fi} \end{bmatrix}, \quad (4)$$

$$\mathbf{S}_f = \begin{bmatrix} 0 \\ M_{fpi} + \alpha_f g_i \\ Q_{fp} \end{bmatrix}. \quad (5)$$

In (2)-(5), α_f , ρ_f , U_{fi} and p_f are fluid-phase volume-fraction, density, velocity components and pressure respectively. The total energy E_f can be written as:

$$E_f = \frac{p_f}{(\gamma - 1)\rho_f} + \frac{1}{2} U_{fj} U_{fj}, \quad (6)$$

where γ is the ratio of specific heats. In (4), the components of the viscous stress tensor σ_{fij} are given by

$$\sigma_{fij} = \mu_f \left(\frac{\partial U_{fi}}{\partial x_j} + \frac{\partial U_{fj}}{\partial x_i} \right) - \frac{2}{3} \mu_f \frac{\partial U_{fk}}{\partial x_k} \delta_{ij}, \quad (7)$$

where μ_f is the fluid dynamic viscosity and δ_{ij} denotes Kronecker delta. The body force due to gravity is accounted for by $\alpha_f g_i$. For the current work, gravity is not considered. The other two source terms, M_{fpi} and Q_{fp} account for momentum and energy exchange between the fluid and particle phases. Details about these two source terms will be discussed in a later section.

Particle-phase governing equations

Kinetic equation. Dilute gas-particle flows can be modeled by a kinetic equation [14, 15, 16] of the form:

$$\partial_t f + \mathbf{v} \cdot \partial_{\mathbf{x}} f + \partial_{\mathbf{v}} \cdot (f \mathbf{F}) = \mathbb{C}, \quad (8)$$

where $f(\mathbf{v}, \mathbf{x}, t)$ is the velocity based number density function, \mathbf{v} is the particle velocity, \mathbf{F} is the force acting on individual particle, and \mathbb{C} is the collision term representing the rate of change in the number density function due to collisions. The collision term can be described using Bhatnagar-Gross-Krook (BGK) collision operator [17]:

$$\mathbb{C} = \frac{1}{\tau_c} (f_{\text{eq}} - f), \quad (9)$$

where τ_c is the characteristic collision time, and f_{eq} is the Maxwellian equilibrium number density function given by:

$$f_{\text{eq}}(\mathbf{v}) = \frac{M^0}{\sqrt{(2\pi\sigma_{\text{eq}})^3}} \exp\left(-\frac{|\mathbf{v} - \mathbf{U}_p|^2}{2\sigma_{\text{eq}}}\right), \quad (10)$$

in which \mathbf{U}_p is the mean particle velocity, σ_{eq} is the equilibrium variance and $M^0 = \int f d\mathbf{v}$ is the particle number density. In fluid-particle flows, the force term is given by the sum of the gravitational contribution and the drag term exerted from the fluid on the particles.

Moment transport equations. In the quadrature-based moment method of Fox, a set of moments of number density function f are transported and their evolution in space and time is tracked. Each element of the moment set is defined through integrals of the velocity distribution function. For the first few moments the defining integrals are:

$$\begin{aligned} M^0 &= \int f d\mathbf{v}, \\ M_i^1 &= \int v_i f d\mathbf{v}, \\ M_{ij}^2 &= \int v_i v_j f d\mathbf{v}, \\ M_{ijk}^3 &= \int v_i v_j v_k f d\mathbf{v}. \end{aligned} \quad (11)$$

In these equations, the superscript of M represents the order of corresponding moment. The particle-phase volume fraction α_p and mean particle velocity \mathbf{U}_p are related to these moments by:

$$\alpha_p = V_p M^0 \quad (12)$$

and

$$\rho_p \alpha_p U_{pi} = m_p M_i^1 \quad (13)$$

where $m_p = \rho_p V_p$ is the mass of a particle with density ρ_p and volume V_p . For 2D cases, $V_p = \pi d_p^2/4$ and for

3D cases, $V_p = \pi d_p^3/6$. Likewise, the particle temperature is defined in terms of the trace of the particle velocity covariance matrix, which is found from M_{ij}^2 and lower-order moments. By definition, $\alpha_p + \alpha_f = 1$ and this relation must be accounted for when solving a fully coupled system for the fluid and particle phases.

Moment transport equations are obtained by applying the definition of moments to (8). The transport equations for moments in (11) can be written as:

$$\frac{\partial \mathbf{W}_p}{\partial t} + \frac{\partial \mathbf{H}_{pl}(\mathbf{W}_p)}{\partial x_l} = \mathbf{D}_p + \mathbf{G}_p + \mathbf{C}_p. \quad (14)$$

In (14), \mathbf{W}_p and $\mathbf{H}_{pl}(\mathbf{W}_p)$ are the conserved moments and spatial fluxes respectively and are given as:

$$\mathbf{W}_p = \begin{bmatrix} M^0 \\ M_i^1 \\ M_{ij}^2 \\ M_{ijk}^3 \end{bmatrix}, \quad (15)$$

$$\mathbf{H}_{pl}(\mathbf{W}_p) = \begin{bmatrix} M_l^1 \\ M_{il}^2 \\ M_{ijl}^3 \\ M_{ijkl}^4 \end{bmatrix}. \quad (16)$$

The source terms on right hand side of (14), \mathbf{D}_p , \mathbf{G}_p and \mathbf{C}_p respectively denote drag, gravity and collision terms and can be written as:

$$\mathbf{D}_p = \begin{bmatrix} 0 \\ D_i^1 \\ D_{ij}^2 \\ D_{ijk}^3 \end{bmatrix}, \quad (17)$$

$$\mathbf{G}_p = \begin{bmatrix} 0 \\ g_i M^0 \\ g_i M_j^1 + g_j M_i^1 \\ g_i M_{jk}^2 + g_j M_{ik}^2 + g_k M_{ij}^2 \end{bmatrix}, \quad (18)$$

$$\mathbf{C}_p = \begin{bmatrix} 0 \\ 0 \\ C_{ij}^2 \\ C_{ijk}^3 \end{bmatrix}. \quad (19)$$

Gravity is not considered in the current work. Hence, $\mathbf{G}_p = 0$. The details of drag and collision terms will be discussed later.

According to the third order QMOM derived by Fox [2, 13], following set of moments are transported in 2D and 3D respectively:

$$\mathbf{W}_p^{2D} = [M^0, M_1^1, M_2^1, M_{11}^2, M_{12}^2, M_{22}^2, M_{111}^3, M_{112}^3, M_{122}^3, M_{222}^3]^T \quad (20)$$

and

$$\mathbf{W}_p^{3D} = [M^0, M_1^1, M_2^1, M_3^1, M_{11}^2, M_{12}^2, M_{13}^2, M_{22}^2, M_{23}^2, M_{33}^2, M_{111}^3, M_{112}^3, M_{113}^3, M_{122}^3, M_{123}^3, M_{133}^3, M_{222}^3, M_{223}^3, M_{233}^3, M_{333}^3]^T. \quad (21)$$

For simplicity, hereinafter we will assume that all of the moments have been multiplied by V_p , so that the zero order moment corresponds to the particle-phase volume fraction i.e. $M^0 = \alpha_p$. This simplification helps in handling of coupling terms.

Quadrature-based closures. Using the BGK model [17], the collision terms in (19) can be closed. Details of closure of collision terms can be found in [4]. However, the set of transport equations in (14) is still unclosed because of the spatial flux and drag terms. Each equation contains the spatial fluxes of the moments of order immediately higher. In quadrature-based moment methods, quadrature formula are used to provide closures to these terms in the moment transport equations, by introducing a set of weights and abscissas. The number density function f is written in terms of the quadrature weights (n) and abscissas (\mathbf{U}_α) using Dirac delta representation:

$$f(\mathbf{v}) = \sum_{\alpha=1}^{\beta} n_\alpha \delta(\mathbf{v} - \mathbf{U}_\alpha). \quad (22)$$

The method based on (22) is called β -node quadrature method. The moments can be computed as a function of quadrature weights and abscissas by using the above definition of f in (7):

$$\begin{aligned} M^0 &= \sum_{\alpha=1}^{\beta} n_\alpha, \\ M_i^1 &= \sum_{\alpha=1}^{\beta} n_\alpha U_{\alpha i}, \\ M_{ij}^2 &= \sum_{\alpha=1}^{\beta} n_\alpha U_{\alpha i} U_{\alpha j}, \\ M_{ijk}^3 &= \sum_{\alpha=1}^{\beta} n_\alpha U_{\alpha i} U_{\alpha j} U_{\alpha k}. \end{aligned} \quad (23)$$

The source terms in (17) due to drag are computed as:

$$\begin{aligned} D_i^1 &= \sum_{\alpha=1}^{\beta} \frac{n_\alpha}{m_p} F_{i\alpha}, \\ D_{ij}^2 &= \sum_{\alpha=1}^{\beta} \frac{n_\alpha}{m_p} (F_{i\alpha} U_{j\alpha} + F_{j\alpha} U_{i\alpha}), \\ D_{ijk}^3 &= \sum_{\alpha=1}^{\beta} \frac{n_\alpha}{m_p} (F_{i\alpha} U_{j\alpha} U_{k\alpha} + F_{j\alpha} U_{k\alpha} U_{i\alpha} + F_{k\alpha} U_{i\alpha} U_{j\alpha}), \end{aligned} \quad (24)$$

where the drag force term $F_{i\alpha}$ is given by

$$F_{i\alpha} = \frac{m_p}{\tau_d} (U_{fi} - U_{i\alpha}). \quad (25)$$

In (25), the drag time τ_d is given by

$$\tau_d = \frac{4d_p \rho_p}{3\alpha_f \rho_f C_d |\mathbf{U}_f - \mathbf{U}_\alpha|}. \quad (26)$$

The drag coefficient C_d is given by Schiller and Nauman correlation [18]:

$$C_d = \frac{24}{\alpha_f \text{Re}_{p\alpha}} [1 + 0.15(\alpha_f \text{Re}_{p\alpha})^{0.687}] \alpha_f^{-2.65}, \quad (27)$$

in which $\text{Re}_{p\alpha} = \rho_f d_p |\mathbf{U}_f - \mathbf{U}_\alpha| / \mu_f$. The coupling source terms for the fluid-phase in (5) are given by:

$$M_{fpi} = \sum_{\alpha=1}^{\beta} \left(\frac{n_\alpha}{V_p} F_{i\alpha} \right), \quad (28)$$

$$Q_{fp} = \sum_{\alpha=1}^{\beta} \left(\frac{n_\alpha}{V_p} F_{i\alpha} U_{i\alpha} \right). \quad (29)$$

The next few sections discuss the details of the fluid and particle phase solvers and the coupling between them. Although, for the numerical simulations a two-stage Runge-Kutta scheme is used, for simplicity, all the discussion on solver details and coupling algorithm will be based on a single-stage time-integration.

Fluid-phase solver

Let I and ∂I denote any cell in the domain and its boundary respectively. Also let $e \in \partial I$ be a face of cell I , A_e be its area and I_{nb_e} be the neighbouring cell corresponding to this face. The finite-volume scheme using single-stage explicit time-integration for (1) can be written as:

$$\begin{aligned} \mathbf{W}_{fI}^{n+1} &= \mathbf{W}_{fI}^n - \frac{\Delta t}{vol_I} \sum_{e \in \partial I} \left\{ \mathbf{G}_f \left(\mathbf{W}_{fe_I}^n, \mathbf{W}_{fe_{I_{nb_e}}}^n \right) A_e \right\} \\ &\quad + \frac{\Delta t}{vol_I} \sum_{e \in \partial I} \left\{ \mathbf{G}_f^v \left(\mathbf{W}_{fe_I}^n, \mathbf{W}_{fe_{I_{nb_e}}}^n \right) A_e \right\} \\ &\quad - \Delta t \mathbf{S}_f, \end{aligned} \quad (30)$$

where \mathbf{W}_{fI}^n and \mathbf{W}_{fI}^{n+1} are the cell averaged values while \mathbf{W}_{feI}^n and $\mathbf{W}_{feI_{nb_e}}^n$ are the values reconstructed on different sides of the face e . Also, vol_I denotes the volume of cell I . In (30), \mathbf{G}_f and \mathbf{G}_f^v denote numerical inviscid and viscous fluxes respectively. Roe flux [19] is used to calculate \mathbf{G}_f . For calculation of viscous flux, gradient of velocity field is required which is obtained using a least-squares linear reconstruction [20, 21]. In the current work, results are presented using 1st-order and 2nd-order finite-volume schemes. For the 1st-order finite-volume scheme, a piecewise-constant reconstruction is used i.e. $\mathbf{W}_{feI}^n = \mathbf{W}_{fI}^n$. For the 2nd-order finite-volume, a least-squares linear reconstruction is obtained using cell averaged values of neighbouring cells. No slip boundary conditions are applied at walls using a ghost-cell approach.

Particle-phase solver

The particle-phase equations evolve the moments due to three kinds of terms - spatial fluxes, collisions and drag. These three terms are treated sequentially using an operator-splitting technique. First the moments are updated using spatial flux terms, then using drag terms and finally using collision terms. A detailed solution algorithm involving all the terms can be found in [1, 4, 13].

Spatial flux terms. Consider a 3D domain. Again, let I and ∂I denote any cell in the domain and its boundary respectively. Also, let $e \in \partial I$ be a face of cell I , A_e be its area and I_{nb_e} be the neighbouring cell corresponding to this face. The finite-volume scheme using single-stage explicit time-integration for the spatial flux terms in (14) can be written as:

$$\mathbf{W}_{pI}^* = \mathbf{W}_{pI}^n - \frac{\Delta t}{vol_I} \sum_{e \in \partial I} \left\{ \mathbf{G}_p \left(\mathbf{W}_{peI}^n, \mathbf{W}_{peI_{nb_e}}^n \right) A_e \right\}, \quad (31)$$

where \mathbf{W}_{pI}^n and \mathbf{W}_{pI}^* are the cell averaged values while \mathbf{W}_{peI}^n and $\mathbf{W}_{peI_{nb_e}}^n$ are the values reconstructed on different sides of the face e . In (31), vol_I denotes the volume of cell I . Let $\hat{\mathbf{n}} = [n_1^{eI} \ n_2^{eI} \ n_3^{eI}]$ denote the outward unit normal for cell I at face e . The numerical flux \mathbf{G}_p

is computed as:

$$\mathbf{G}_p \left(\mathbf{W}_{peI}^n, \mathbf{W}_{peI_{nb_e}}^n \right) = \sum_{\alpha=1}^{\beta} \left\{ \begin{pmatrix} n_{\alpha} \\ n_{\alpha} U_{i\alpha} \\ n_{\alpha} U_{i\alpha} U_{j\alpha} \\ n_{\alpha} U_{i\alpha} U_{j\alpha} U_{k\alpha} \end{pmatrix} U_n^+ \right\}_{eI} + \sum_{\alpha=1}^{\beta} \left\{ \begin{pmatrix} n_{\alpha} \\ n_{\alpha} U_{i\alpha} \\ n_{\alpha} U_{i\alpha} U_{j\alpha} \\ n_{\alpha} U_{i\alpha} U_{j\alpha} U_{k\alpha} \end{pmatrix} U_n^- \right\}_{eI_{nb_e}} \quad (32)$$

where $U_n^+ = \max(U_{1\alpha} n_1^{eI} + U_{2\alpha} n_2^{eI} + U_{3\alpha} n_3^{eI}, 0)$ and $U_n^- = \min(U_{1\alpha} n_1^{eI} + U_{2\alpha} n_2^{eI} + U_{3\alpha} n_3^{eI}, 0)$. In the current work, results are presented using 1st-order and *quasi*-2nd-order [5, 6] finite-volume schemes. For the 1st-order finite-volume scheme, a piecewise-constant reconstruction is used for both weights and abscissas. For the *quasi*-2nd-order finite-volume, a least-squares linear reconstruction [20, 21] is used for weights while for abscissas, a piecewise-constant reconstruction is used. Moreover, a limiter [20, 22] is applied to the least-squares reconstruction of weights to avoid spurious oscillations. Wall boundary conditions as described in [4] are applied using a ghost-cell approach.

Collision terms. Collisions only affect the second and third order moments. These moments are updated using BGK model as:

$$\mathbf{W}_{pI}^{**} = \Delta_{pI}^* + (\mathbf{W}_{pI}^* - \Delta_{pI}^*) \exp(-\Delta t / \tau_c), \quad (33)$$

where τ_c is the collision time and Δ_{pI} denotes the set of equilibrium moments. Details about the calculation of τ_c and Δ_{pI} can be found in [4].

Drag terms. Drag terms do not affect the weights because they do not change the number of particles. The weights obtained after accounting for collisions in (33) are updated using:

$$U_{i\alpha}^{n+1} = U_{i\alpha}^{**} + \Delta t \frac{F_{i\alpha}^{**}}{m_p}. \quad (34)$$

Coupling algorithm

The coupling between fluid and particle phase solvers is obtained by following the underlying steps:

1. Initialize parameters and flow variables for both fluid-phase and particle-phase solvers.
2. For the fluid-phase solver calculate Δt_f using a pre-specified value of CFL.

3. Pass Δt_f , ρ_f , μ_f , \mathbf{U}_f from fluid-phase solver to particle-phase solver.
4. For the particle-phase solver calculate Δt_p . Details of calculation of Δt_p can be found in [6].
5. Calculate global time step, $\Delta t = \min(\Delta t_f, \Delta t_p)$.
6. Advance particle-phase solver by Δt .
 - a) Advance moments by Δt due to spatial flux terms using a finite-volume approach.
 - b) Advance moments by Δt due to collision terms.
 - c) Advance weights by Δt due to drag force terms and compute the coupling source terms M_{fp_i} and Q_{fp} for fluid-phase solver.
7. Pass Δt , M_{fp_i} , Q_{fp} and $\alpha_f (= 1 - \alpha_p)$ from particle-phase solver to fluid-phase solver.
8. Advance fluid-phase solver by Δt .
9. Repeat steps 2 through 8 at each timestep.

Numerical Results

Numerical results are presented for a dilute gas-particle flow in a lid-driven cavity. The lid has a length L and moves with a constant velocity U_{lid} , as schematized in Figure 1. The cavity is filled with the gas phase and with initially uniformly distributed particles. Both the phases have zero initial velocity as initial condition. The evolution of the flow fields are tracked for a time sufficient to the lid to go through twenty lid lengths. The parameters that characterize the system are the Knudsen number (Kn), the Reynolds number (Re), the Stokes number (St) and the mass loading (λ). The Knudsen number is defined as:

$$Kn = \frac{d_p}{6\alpha_p L \sqrt{2}}. \quad (35)$$

The Reynolds number is defined on the base of the lid length and the lid velocity as:

$$Re = \frac{\rho_f |U_{lid}| L}{\mu_f}. \quad (36)$$

The mass loading is given by the ratio

$$\lambda = \frac{\alpha_p \rho_p}{\alpha_f \rho_f}, \quad (37)$$

while Stokes number is defined as:

$$St = \frac{1}{18} \frac{\rho_p}{\rho_f} \left(\frac{d_p}{L} \right)^2 Re. \quad (38)$$

Results are presented for the case with $Kn = 1$, $St = 1$, $Re = 100$, $\lambda = 2.5$. This case is of particular interest as

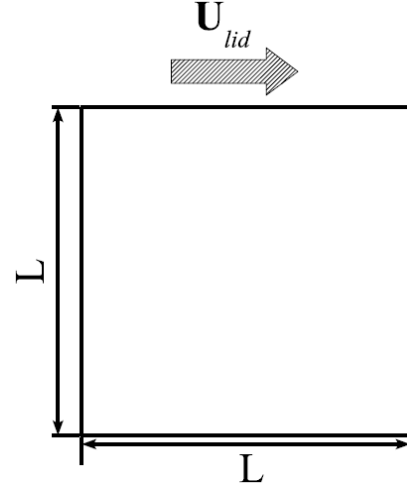


Figure 1: Schematic representation of lid-driven cavity.

it involves particle trajectory crossing which cannot be captured by two-fluid models [3]. Particles are driven by the fluid velocity field. At the top-right corner particles hit the wall and are reflected back. Because of particles with opposing velocities, trajectory crossing occurs near the top-right corner. Figure 2 shows the grid with rectangular cells near the boundary and triangular cells in the core region. Total number of cells is 6904. A two stage Runge Kutta scheme is used for time-integration. Figure 3 and Figure 4 show particle volume-fraction fields at the final time. Figure 3 shows results when 1st-order finite-volume scheme is used for both fluid and particle phase solvers while Figure 4 shows results when 2nd-order finite-volume scheme is used for fluid-phase solver and *quasi*-2nd-order [5, 6] finite-volume scheme is used for particle-phase solver. Both Figure 3 and Figure 4, show the trajectory crossing near the top-right corner. The results are in agreement with the ones presented in [3]. Second-order finite-volume solver for the fluid phase gives better resolution of the fluid velocity field. As the particles are driven by the fluid velocity field, a second-order finite-volume solver for fluid-phase leads to better prediction of particle volume-fraction. The use of *quasi*-2nd-order finite-volume scheme for particle-phase further improves the solution.

Conclusions

In the current work, a compressible finite-volume fluid solver is coupled with a particle-phase solver based on third-order QMOM on unstructured grids. The fluid and particle-phase are fully coupled by accounting for the volume displacement effects induced by the presence of the particles and the momentum exchange between the phases. High-order realizable finite volume schemes are

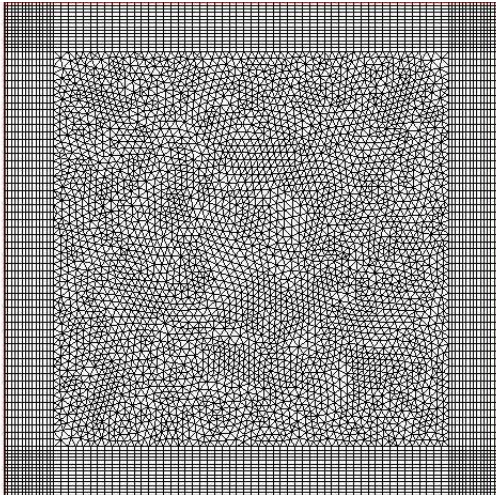


Figure 2: Grid (6904 cells).

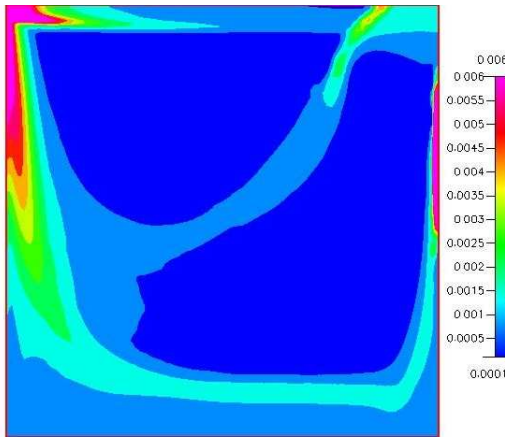


Figure 3: Particle-phase volume-fraction using 1st-order finite-volume solver for both fluid and particle phases.

used for particle-phase QMOM solver. Numerical results are presented for a dilute gas-particle flow in a lid-driven cavity. Complex features like particle-trajectory crossing are captured easily. The coupling can be extended to practical problems as it is relatively inexpensive compared to Lagrangian and direct kinetic solvers.

Acknowledgements

The study was funded by NSF grant CISE-0830214. The views and conclusions herein are those of the authors and should not be interpreted as necessarily representing the official policies or endorsements, either expressed or implied, of NSF or the U.S. Government.

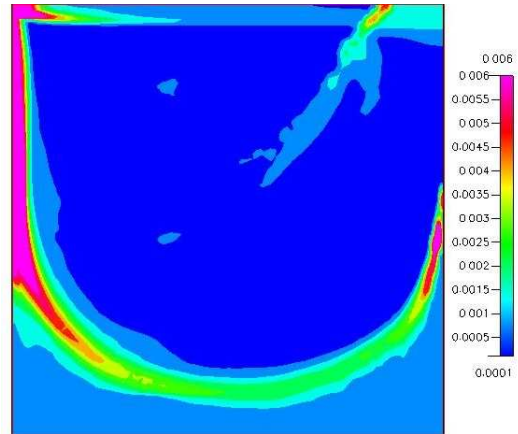


Figure 4: Particle-phase volume-fraction using 2nd-order finite-volume solver for fluid-phase and *quasi*-2nd-order finite-volume solver for particle phase.

References

- [1] O. Desjardins, R.O. Fox, P. Villedieu, A quadrature-based moment method for dilute fluid-particle flows, *Journal of Computational Physics* 227 (2008) 2514-2539.
- [2] R.O. Fox, A quadrature-based third-order moment method for dilute gas-particle flows, *Journal of Computational Physics* 227 (2008) 6313-6350.
- [3] R. Garg, A. Passalacqua, S. Subramaniam, R.O. Fox, A fully coupled quadrature-based moment method for dilute to moderately dilute fluid-particle flows, *Chemical Engineering Science*, 65 (7) (2010) 2267-2283.
- [4] A. Passalacqua, R.O. Fox, R. Garg, S. Subramaniam, Comparison of Euler-Euler and Euler-Lagrange simulations of finite-Stokes-numbers gas-particle flows in a lid-driven cavity, *AICHE Annual Meeting*, Philadelphia (2008).
- [5] V. Vikas, Z.J. Wang, A. Passalacqua, R.O. Fox, Development of High-Order Realizable Finite-Volume Schemes for Quadrature-Based Moment Method, *AIAA Paper* 2010-1080 (2010).
- [6] V. Vikas, Z.J. Wang, A. Passalacqua, R.O. Fox, Realizable High-Order Finite-Volume Schemes for Quadrature-Based Moment Method, *Journal of Computational Physics*, submitted for publication.
- [7] A.E. Beylich, Solving the kinetic equation for all Knudsen numbers, *Physics of Fluids* 12 (2000) 444-465.

- [8] Y. Ogata, H.-N. Im, T. Yabe, Numerical method for Boltzmann equation with Soroban-grid CIP method, *Communications in Computational Physics* 2 (4) (2007) 760-782.
- [9] G.A. Bird, *Molecular Gas Dynamics and the Direct Simulation of Gas Flows*, Clarendon, Oxford, 1994.
- [10] H. Enwald, E. Peirano, A.E. Almstedt, Eulerian two-phase flow theory applied to fluidization, *International Journal of Multiphase Flow* 22 (1996) 21-66.
- [11] D.L. Marchisio, R.O. Fox, Solution of population balance equations using the direct quadrature method of moments, *Journal of Aerosol Science* 36 (2005) 43-73.
- [12] R.O. Fox, Optimal Moment Sets for Multivariate Direct Quadrature Method of Moments, *Industrial & Engineering Chemistry Research* 48 (21) (2009) 9686-9696.
- [13] R.O. Fox, Higher-order quadrature-based moment methods for kinetic equations, *Journal of Computational Physics* 228 (2009) 7771-7791.
- [14] C. Cercignani, *The Boltzmann Equation and its Applications*, Springer, New York, 1988.
- [15] S. Chapman, T.G. Cowling, *The Mathematical Theory of Nonuniform Gases*, Cambridge University Press, Cambridge, 1970.
- [16] H. Struchtrup, *Macroscopic Transport Equations for Rarefied Gas Flows*, Springer, New York, 2005.
- [17] P.L. Bhatnagar, E.P. Gross, M. Krook, A model for collision processes in gases. I. Small amplitude processes in charged and neutral one-component systems, *Physical Reviews* 94 (1954) 511-525.
- [18] L. Schiller, A. Nauman, A drag coefficient correlation, *V.D.I. Zeitung* 77 (1935) 318-320.
- [19] P. Roe, Approximate Riemann Solvers, Parameter Vectors, and Difference Schemes, *Journal of Computational Physics*, 43 (1981) 357-372.
- [20] T.J. Barth, D.C. Jespersen, The design and application of upwind schemes on unstructured meshes, *AIAA Paper* 89-0366 (1989).
- [21] T.J. Barth, P.O. Frederickson, High-order solution of the Euler equations on unstructured grids using quadratic reconstruction, *AIAA Paper* 90-0013 (1990).
- [22] S.K. Godunov, A finite-difference method for the numerical computation of discontinuous solutions of the equations of fluid dynamics, *Math Sbornik*, 47 (1959) 271-306.